Supplementary Material

The `Results-plotter` function enables visualization of the model predictions for specific cases, allowing for direct comparison with the observed data. Two representative years—1986 and 1998—have been selected for this purpose and are illustrated in Fig. S1 and Fig. S2, respectively.

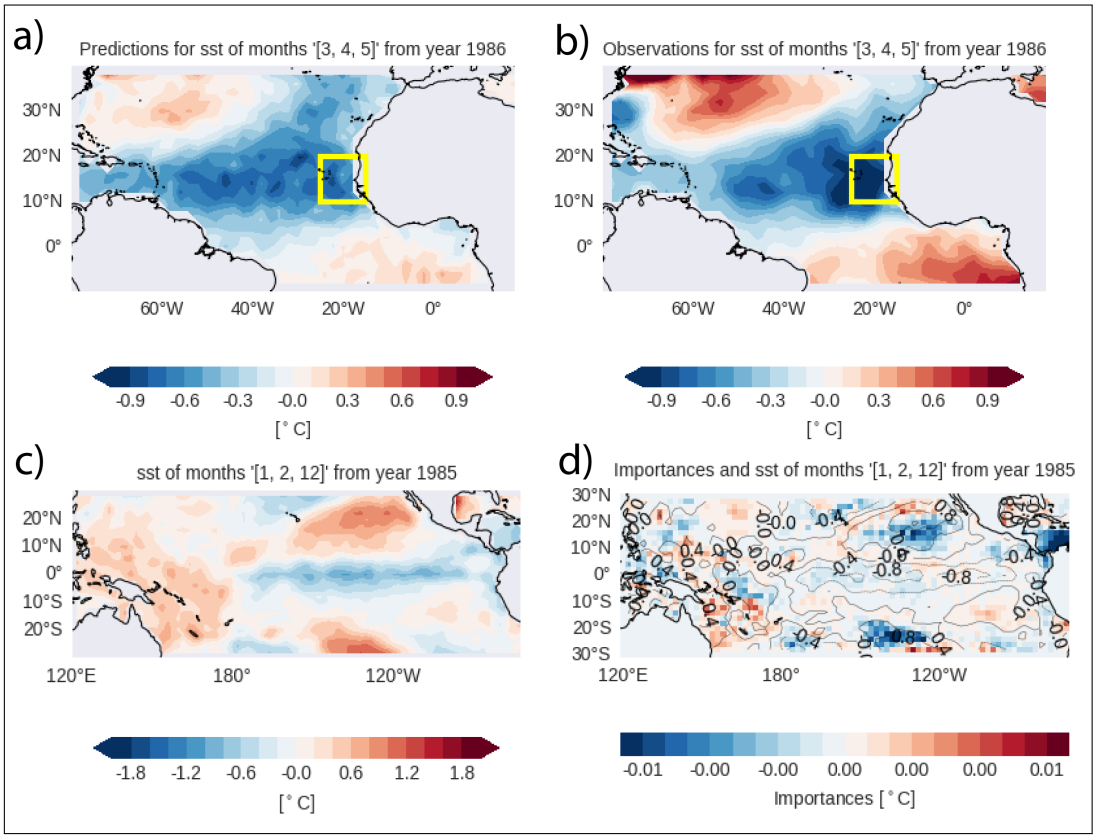

Figure S1. Comparison of model predictions for a specific sample year. Panels show: (a) predicted MAM Atlantic SST anomalies (°C); (b) observed MAM Atlantic SST anomalies (°C) for the year 1986; (c) Pacific SST during DJF (°C) for the year 1985 used as the predictor field; and (d) Pacific SST DJF predictor field for the 1985 sample, with contours (°C) representing SST values and shaded areas (°C) indicating the model attributions for the selected predictand region (yellow box in panels a and b). The yellow box marks the target region where model attributions are computed.

The first case presented (Fig. S1) corresponds to a central La Niña event, characterized by negative SST anomalies in the central equatorial Pacific, along with positive anomalies over the Warm Pool and subtropical regions of the Pacific Ocean. In this scenario, the model predicted a cooling of the Tropical North Atlantic (TNA) and the MSCU region, as well as a warming over the eastern equatorial Atlantic and the Gulf Stream region. To gain insight into how the model made these predictions, we focused on the MSCU region (highlighted by a yellow box in Fig. S1a and Fig. S1b and computed the Integrated Gradients

attributions for the 1986 prediction. These attributions are shown in Fig. S1d). The importance values are expressed in units of the predicted variable (°C), which in this case matches the units of the predictor (SST anomalies). The attribution map reveals the individual contribution of each SST predictor to the prediction over the region marked by the yellow box. Notably, both the Caribbean region and the warming zones in the central tropical Pacific greatly contributed to the prediction of negative SST anomalies in the Mauritanian-Senegalese Coastal Upwelling region.

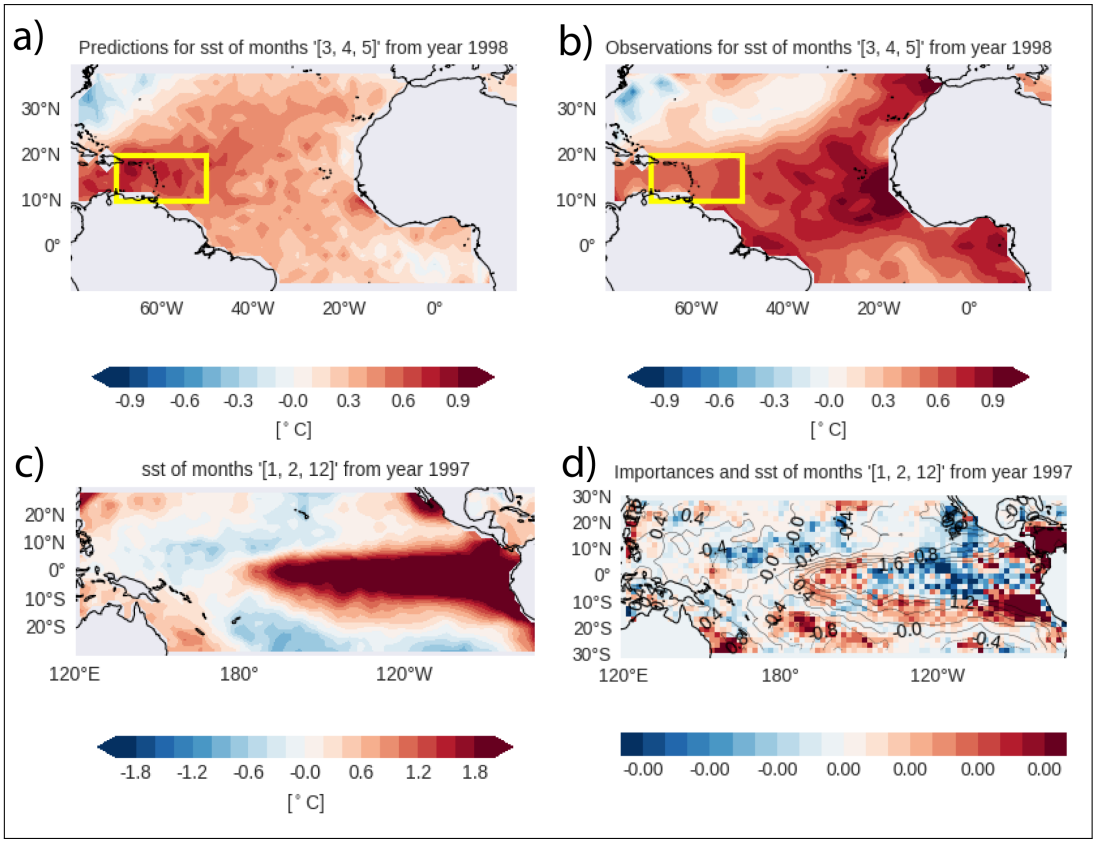

Figure S2. Comparison of model predictions for a specific sample year. Panels show: (a) predicted MAM Atlantic SST anomalies (°C); (b) observed MAM Atlantic SST anomalies (°C) for the year 1998; (c) Pacific SST during DJF (°C) for the year 1997 used as the predictor field; and (d) Pacific SST DJF predictor field for the 1997 sample, with contours (°C) representing SST values and shaded areas (°C) indicating the model attributions for the selected predictand region (yellow box in panels a and b). The yellow box marks the target region where model attributions are computed.

Figure S2 illustrates the second case, corresponding to a canonical El Niño event in 1998, associated with widespread warming in the tropical Atlantic, including the TNA region. In this case, the model accurately reproduced the observed warming signal. For the attribution analysis, we selected a classic TNA index region, delineated by the yellow box in Fig. S2a) and Fig. S2b). The attribution map for this case is somewhat noisier compared to the 1986 scenario. Nevertheless, some consistent patterns emerge: there are positive contributions from the Caribbean, the central Pacific, and a latitudinal band south of

20 10°S. In contrast, negative contributions are found mainly in the Niño 3 region and certain areas north of 10°N, which act to counterbalance the warming signal.

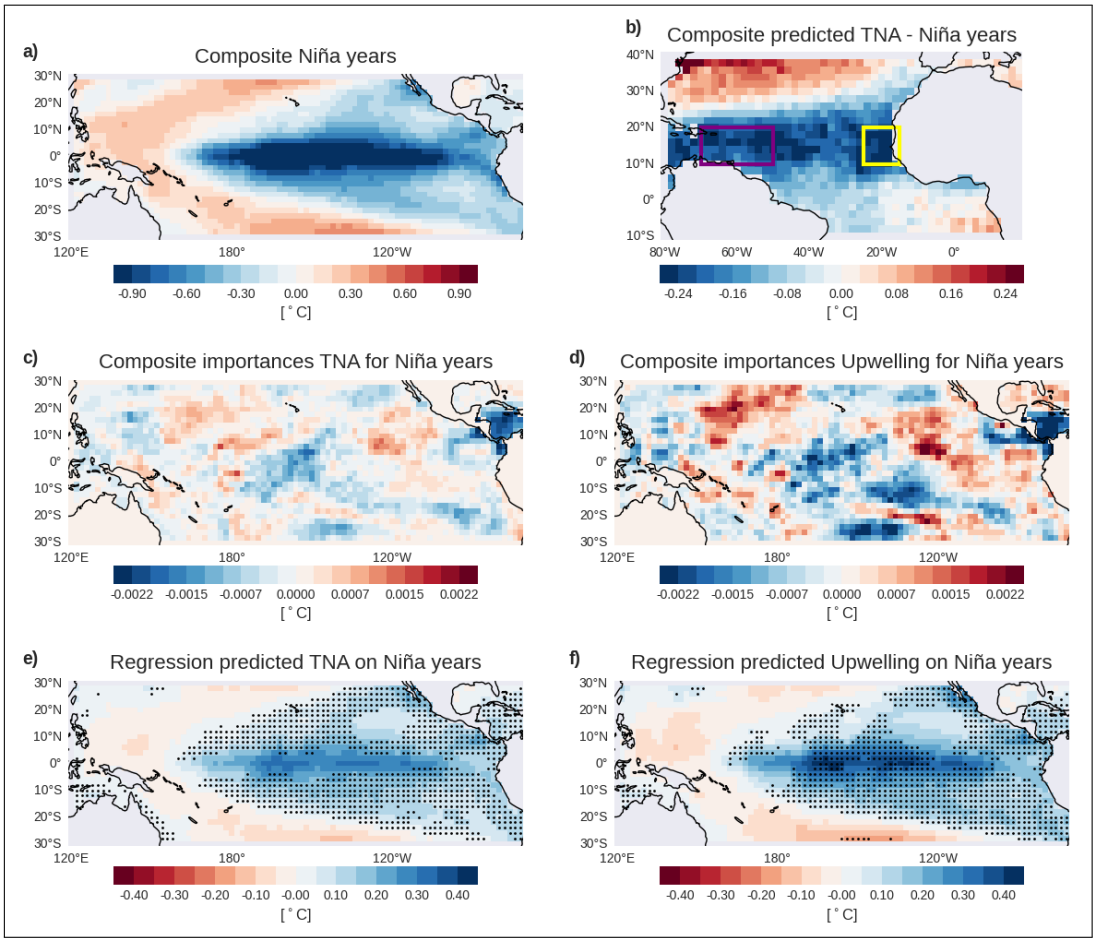

Figure S3. Composite of model predictions corresponding to Niña events. Panels show: (a) observed Pacific SST anomalies during DJF; (b) predicted Atlantic SST anomalies during MAM; (c) attribution maps over the predictor field related to the western Tropical North Atlantic (WTNA) region predictions (purple box shown in panel b); (d) attribution maps over the predictor field related to the upwelling region predictions (yellow box shown in panel b); (e) regression of the TNA index on Pacific DJF SST; and (f) regression of the upwelling index on Pacific DJF SST. The stippling in panels (e) and (f) indicates regions where the regression is significant at the 95% confidence level, according to a Monte Carlo two-tailed significance test. Attribution maps (c) and (d) represent the relative contribution of each grid point in the predictor field to the forecasted value in the target region. Note that the sum of the attribution values within each map equals the predicted anomaly in the corresponding region (i.e., the sum of values in panel c matches the WTNA anomaly within the purple box in panel b).

Additionally, as was done for El Niño events, we computed the composite for the years in which a La Niña event occurred, based again on the Niño 3.4 index. The result is shown in Figure S3, which, similar to the corresponding El Niño figure, includes the attribution composites for the two study regions. A comparison between both figures reveals a generally similar

behavior, though with opposite signs. However, some areas of particular interest stand out in the case of La Niña, such as a strong contribution from the central Pacific to cooling and a meridional dipole in the Caribbean Sea.

The regression analysis based on the first observed principal component of European precipitation during OND (Fig. S4) reveals SST anomaly patterns in the Pacific consistent with those obtained using the predicted PC1 (see Fig. 6). Concretely, during the low-skill period from 1914 to 1941, the SST pattern resembles a weak, more central-Pacific Niño type, whereas the late low-skill period (1970–2007) exhibits a more intense and eastern-Pacific Niño pattern. In contrast, the high-skill interval (1942–1969) is characterized by a stronger eastern-Pacific Niña-type SST pattern. Significant atmospheric responses in the Z200 are only observed during this high-skill period, where the response resembles a Gill-type pattern associated with ENSO, along with the propagation of Rossby waves. Specifically, the atmospheric response in Z200 during this period takes the form of a circumglobal wave pattern, highlighting the strong teleconnection. Conversely, the earlierlow-skill period show weaker Z200 responses.

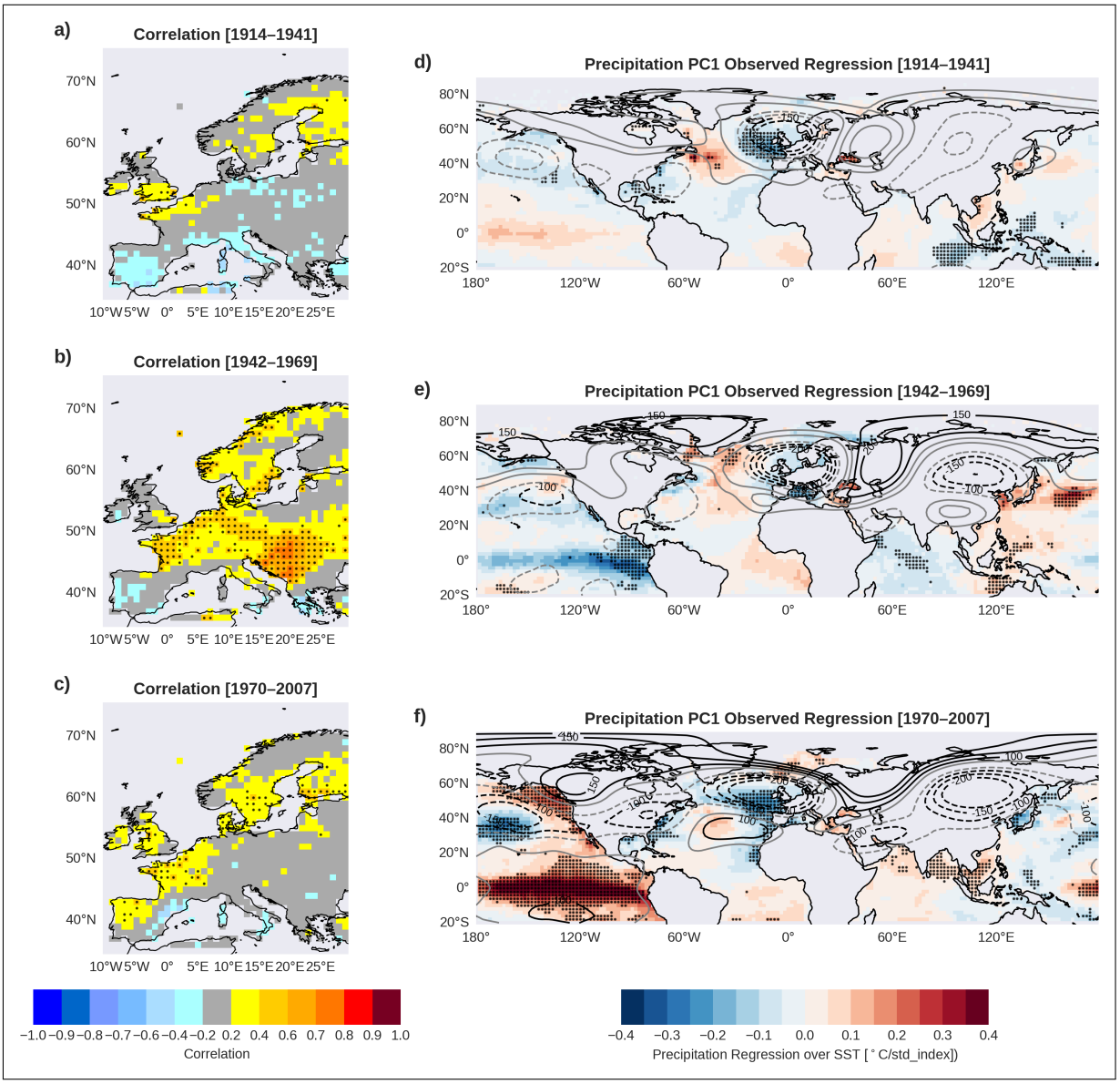

Figure S4. Panel of correlation maps between predicted and observed precipitation anomalies over Europe during OND for three distinct periods: (a) 1914–1941, (b) 1942–1969, and (c) 1970–2007. Data points indicate grid cells where the correlation is statistically significant at the 95% confidence level based on a t-test. The panel also includes regression maps of the first observed principal component (shown in blue in 5c) onto the SST (shaded) and 200 hPa geopotential height (Z200; contour) fields during OND. Statistical significance of the regressions is indicated by stippling over the SST maps and black contour lines over the Z200 maps, according to a Monte Carlo test at the 95% confidence level.